*** Author postprint ***

Many-to-one function of cat-like mandibles highlights a continuum of sabre tooth adaptions

https://doi.org/10.1098/rspb.2022.1627

Narimane Chatar[1,*], Valentin Fischer[1], Z. Jack Tseng[2]

[1] Evolution & Diversity Dynamics lab, UR Geology, Université de Liège, Building B18, Quartier Agora, Allée du Six Août 14, 4000 Liège, Belgium NC 0000-0003-0449-8574, VF 0000-0002-8808-6747
[2] Department of Integrative Biology and Museum of Paleontology, University of California, Berkeley, CA 94720, United States 0000-0001-5335-4230

* Corresponding author: narimane.chatar@uliege.be

Abstract

Cat-like carnivorans are a textbook example of convergent evolution with distinct morphological differences between taxa with short or elongated upper canines, the latest being often interpreted as an adaptation to bite at large angles and subdue large prey. This interpretation of the sabretooth condition is reinforced by a reduced taxonomic sampling in some studies, often focusing on highly derived taxa or using simplified morphological models. Moreover, most biomechanical analyses focus on biting scenarios at small gapes, ideal for modern carnivora but ill-suited to test for subduction of large prey by sabre-toothed taxa. In this contribution we present the largest 3D collection-based muscle-induced biting simulations on cat like carnivorans by running a total of 1,074 analyses on 17 different taxa at three different biting angles (30°, 60° and 90°) including both morphologies. While our results show a clear adaptation of extreme sabre-toothed taxa to bite at larger angles in terms of stress distribution, other performance variables display surprising similarities between all forms at the different angles tested, highlighting a continuous rather than bipolar spectrum of hunting methods in cat-like carnivorans and demonstrating a wide functional disparity and nuances of the sabretooth condition that cannot simply be characterized by specialized feeding biomechanics.

Keywords: Finite element analysis, biting simulation, Felidae, Nimravidae, mandible biomechanics, Carnivora

Cite as: Chatar, N., Fischer, V., & Tseng, Z. J. (2022). Many-to-one function of cat-like mandibles highlights a continuum of sabre-tooth adaptations. *Proceedings of the Royal Society B: Biological Sciences 289*:20221627. http://doi.org/10.1098/rspb.2022.1627

Introduction

A vast series of vertebrate clades have independently evolved sabretooth morphologies [1–4]. However, the biomechanical consequences of this trait is poorly known. In cat-like clades (Felidae, Nimravidae, and Thylacosmilidae) [5–10], both sabretoothed and non-sabretoothed cat-like carnivoran morphotypes are textbook examples of convergent evolution with their own suite of craniomandibular adaptations [3,11–13], the sabretooth morphology being often interpreted as an adaptation for subduing large prey [5–10]. However, functional anatomy remains blur and, at first; similar ecomorphologies were suggested for all sabre-tooths clade before some authors highlighted the functional differences between scimitar-toothed and dirk-toothed taxa and, besides, some lineage are extremely convergent with modern “conical” tooth felids (Metailurini and Nimravini) [3,7,11,14,15]. Different hunting behaviours were already proposed for dirk- and scimitar-toothed machairodontines based on FEA simulations [15] but some species considered as ‘mosaic taxa’ (e.g., *Xenosmilus hodsonae* [12]), complexified those models linking form and function. Lautenschlager *et al*. (2020) [16] recently highlighted the diversity of mechanical behaviours among sabretooth mandibles suggesting that homotherins and metailurins might have use a different bite than smilodontins. Based on a mandibular shape extremely similar to that of extant felines it was also suggested that primitive machairodontine (*Machairodus aphanistus* and *Promegantereon ogygia*) might also have used a different bite than more derived sabretoothed felids [17]. While long-toothed taxa have been widely studied in terms of bending resistance, tooth morphology, gape, and post-cranial anatomy [8,10,12,15,16], taxa with shorter canines are often left out of comparative analyses.

The very first study computing finite element analysis including on cat-like carnivorans was published by McHenry *et al*. (2007) [18] comparing *Smilodon fatalis* to *Panthera leo* and shown that *Smilodon* head and neck were the most efficient on a restrained prey and concluded that prey had to be brought to ground before bite. Then, a first attempt of comparing numerous cat-like carnivorous mammals mechanical performances using FEA was made by Piras *et al*. (2013) [19] using 2D spline approximation reconstructed from Procrustes coordinates from their geometric morphometric analysis. They found out that sabre-toothed mandibles were more stressed than in modern felines mainly in the ascending ramus [19]. Later, a dirk- and scimitar-toothed cats comparison was published by Figueirido *et al.* (2018) [15] comaring *Smilodon fatalis* and a *Homotherium serum* skulls, highlighting high variations between those two machairodontine morphotypes. A comparison between *Smilodon* and *Thylacosmilus* shown that the placental sabretooth might not have been the fearsome predator it was

thought to be but more of a scavenger Janis *et al*. (2020) [20]. Finally, Lautenschlager *et al*. (2020) [16] published a large-scale 2D study comparing all mammalian and non-mammalian sabretooths based on two-dimensional outlines using FEA, gape analysis and geometric morphometric. Their results highlighted the high intra and inter clade functional diversity among sabretooths predators and is thus an interesting starting point for further analysis [16]. However, biomechanical simulations on carnivorans are often run at gape angle ranging from 25 to 30° a classical angle for modern carnivora [21] that is however ill-suited to test for subduction of large prey by sabre-toothed taxa.

For the first time we computed three dimensional biomechanical simulations on a large dataset testing different gape angles including highly derived sabretooth taxa (e.g. *Barbourofelis fricki*, *Babrourofelis loveorum*, *Smilodon fatalis*, *Homotherium crenatidens* or *Hoplophoneus primaevus*) but also early machairodontine taxa (e.g. *Paramachaerodus orientalis* and *Machairodus aphanistus*), machairodontines/nimravines taxa which have fairly short upper canines (e.g. *Yoshi minor*) and a wide range of extant felines, in a comparative framework. We also tested different gape angles by performing our analyses at three different gapes: 30°, 60° and 90.

Here, we thoroughly analyse the biting biomechanics of sabre-toothed and non-sabre-toothed taxa by applying Finite Element Analyses (FEA) on the largest dataset ever assembled of cat-like placental mandible 3D models, under a variety of gape scenarios. We would have expected taxa with the longest upper canines to be more efficient at larger angles and thus to observe an improvement in the measured performance variables. However, while our results show a clear adaptation of extreme sabre-toothed taxa to bite at larger angles in terms of von Mises stress, other performance variables display surprising similarities between sabretoothed and non-sabretoothed forms. The similarities of some performance variables show that the cat like mandible is an example of ‘many-to-one mapping’ of form-function relationships where forms with obvious morphological disparity produce the same function.

Material and Methods

Taxonomic sampling

A total of 19 mandibles from 17 different taxa were used to compute the analyses, the complete list of specimens with their metadata is available in Table 1.

Table 1: Specimens used to compute the FE analyses. Institutional abbreviations: **AMNH** American museum of Natural History (New York, USA), **DNMNH** Ditsong National Museum of Natural History (Pretoria, South Africa), **PMU** Paleontological Museum Uppsala universitet (Uppsala, Sweden), **UCMP** University of California Museum of Paleontology, **FAVE Lab** Functional anatomy and vertebrate evolution Lab (Berkeley USA), **NHMLA**: Natural History Museum of Los Angeles County (Los Angeles, USA), **NHMUK**: Natural History Museum (London, UK), **MNHN** Muséum National d'histoire Naturel (Paris, France), **NRM** Naturhistoriska riksmuseet (Stockholm, Sweden), **UF** University of Florida (Gainesville, USA). Upper canine ratio = length of the upper canine/cranial length.

Subfamily	Species	Upper canine ratio	Cranial length (mm)	Specimen n°	Age	Holding institution
Felinae	*Caracal caracal*	0.12	110.01	A58401	Extant	NRM
	Lynx rufus	0.13	81.51	FAVE09	Extant	FAVE Lab
	Panthera pardus	0.15	175.25	AMNH 113745	Extant	AMNH
	Panthera onca	0.17	217.53	MNHN-ZM-MO-2006-641	Extant	MNHN
	Panthera tigris	0.17	315.68	MNHN-ZO-AC-1931-60	Extant	MNHN
	Prionailurus rubiginosus	0.12	83.74	MNHN-ZM-MO-2012-54	Extant	MNHN
Machairodontinae	*Amphimachairodus palanderi*	0.26	271.98	PMU 21831	Late Miocene	PMU
	Dinofelis barlowi	0.23	257.07	DNMNH-BF-55-23	Early Pliocene	DNMNH
	Homotherium crenatidens	0.30	330.36	MNHN.F.PET2000	Early Pleistocene	MNHN
	Machairodus aphanistus	0.28	336.27	NHMUK-PV-M37356	Late Miocene	NHMUK
	Paramachaerodus orientalis	0.20	174.74	NHMUK PV M 8959b	Late Miocene	NHMUK
	Smilodon fatalis	0.49	330.72	AMNH-14349	Late Pleistocene	AMNH
	Yoshi minor	0.19	149.52	PMU 21766/2	Late Miocene	PMU
Nimravinae	*Hoplophoneus primaevus*	0.34	170.55	LACM-42890	Late Eocene	NHMLA
	Dinictis felina	0.26	160.70	LACM-162986	LateEocene-Mid Oligocene	NHMLA
Barbourofelinae	*Barbourofelis fricki*	0.74	289.09	UCMP-124942	Late Miocene	UCMP
	Barbourofelis loveorum	0.35	258.04	UF-VP-36855	Late Miocene	UF

Preparation of the 3D data

Estimations of the insertion sites of the three main masticatory muscle groups (m. masseter, m. temporalis and m. pterygoideus) requires the cranium and mandible in articulation. However, the cranium of some fossil species may be missing, crushed, or incomplete. In these situations where the cranial insertion sites could not be unambiguously placed on the associated skull, we used a cranium belonging to another conspecific or congeneric specimen to get the focal coordinates of muscle origins (see Table S1). As routinely employed in FE analyses (e.g. [23–28]), we reconstructed or retrodeformed some models of fossil taxa. To assure transparency, a complete description of the various reconstruction and retro-deformation steps undertaken is available in Figures S1-S9. We first computed FEA on two CT-scan based models and then compared our results to those obtained on the same models from which we cleared the internal anatomy to simulate a surface scan-based model. Our results on both type of models were extremely consistent in terms of von Mises stress, mechanical efficiency and adjusted strain energy (see ESM, Table S2, Figure S10-S11) therefore we used only surface scan-based model for the rest of our analysis, this also get in line with some recent results showing that surface scans might be a good alternative for CT scans in FEA [29]. The CT-scanned specimens used for the comparison were *Lynx rufus* FAVE09 and *Panthera pardus* AMNH-113745. The CT scan for *Lynx rufus* FAVE09 was obtained from the University at Buffalo Clinical and Translational Science Institute Imaging Center on a GE Discovery 690 PET-CT scanner. The scans of *Panthera pardus* AMNH-113745 and *Smilodon fatalis* AMNH-14349 were initially published in [25] and were scanned in the AMNH Microscopy and Imaging Facility on a General Electric high resolution X-ray micro-CT scanner. For CT scanning parameters see Table S3. Image stacks were imported in Avizo lite 2020 (Thermo Fisher Scientific, United States) and region of interest were segmented and exported in STL (STereoLithography) format. Most of the surface scans were obtained with a Creaform HandySCAN 300 laser surface scanner with a resolution varying from 0.2 to 0.5mm (See Table S4). Raw surface scans were then treated using the VX Models software (Creaform, United States) and GeoMagic wrap 2020 (3D Systems, United states) then each part was exported in STL. We measured functional ratios that are commonly considered as sabretooth features: coronoid process height and the upper canine length; using the GOM Inspect suite 2018 (Gesellschaft für Optische Messtechnik, Germany, 2018). (See ESM and Figure S12).

Then, each 3D model was imported in Geomagic Wrap 2020 (3D Systems, United states) and processed. Mandibles were decimated to approximately 150 000 triangles (see Table S5) and their XYZ coordinate systems were

standardized. Models of the cranium and mandible were articulated at 30°, 60°, and 90° of gape angle, providing three biting scenarios for each specimen. On each mandible three muscles groups (*M. temporalis*, *M. masseter*, and *M. pterygoideus* groups) were drawn on each side (6 muscle attachment regions in total) using GeoMagic (Figure S13).

Meshing and FEA protocol

To estimate the forces (Newtons) pulling each muscle insertion, the insertion area (mm^2) was multiplied by 0.3N/mm^2 based on the maximum tension produced by mammalian muscle fibres [30]. All biting simulations were unilateral (left and right side were simulated in different scenarios) so to compensate the balancing side muscle forces were multiplied by 0.6 of working side muscles, following [31]. All mandibles were considered isotropic material; a young's modulus of 18 GPa and a Poisson's ratio of 0.3 were defined according to [32–35].

Solid meshes of the mandibles were generated in the Strand7 FE analysis software (Strand7 Pty Ltd, Australia) using four-noded tetrahedral 'brick' elements after an automated mesh 'cleaning' to remove any duplicated nodes. For each specimen, we produced three solid meshes with a coarse-, a medium- and a fine-resolution, respectively, following [26]. Forces were distributed on the muscle insertions in a tangential traction scenario implemented in the Boneload MATLAB routine written by [36] which we slightly modified to adjust the pressure magnitude. The nodal constraint created on the tip of each tooth to simulate each bite scenarios was restrained in the three axes. To avoid free-body movement or over-constraint of the models [37], a nodal constraint was added on each of the temporomandibular joints (TMJ) preventing any dorsoventral or rostrocaudal movement but still allowing a certain degree of bending of both hemimandibles one towards the other in the mediolateral axis. Then, the linear static solver provided in Strand7 was used to solve the muscle loading model. For model comparison we extracted different performance variables: the mechanical efficiency, adjusted strain energy and von Mises stress (see ESM for more details about the performance variables and the corrections applied to account for allometric variation in the dataset). Finally, the 'graph' tool in Strand7 was used to measure VM stress values across the mandibles by drawing a line from the middle of the symphyseal region to the base of the coronoid process on both the balancing and working side to obtain values over the whole bone while avoiding areas of unrealistic high stress values near nodal constraints. Then we plotted the rolling mean with a window width of 10 to visualise the evolution of VM stress more smoothly. The elongation of the upper canines and the reduction of the coronoid process are key, convergently evolved sabretooth characters [3]. While elongated upper

canines is the most striking sabretooth trait it implies a reduction of the coronoid process for the animal to open its jaw at a larger angle in order to clear the elongated upper canines to bite. We looked at the potential correlation between those two typical sabretooth features and the VM stress using linear regressions (see ESM for more details).

The three different gape angles, using three different mesh resolutions, as well as on three to four different biting points (depending on the number of teeth) on 19 specimens resulted in a total number of analyses of 1,074. All the plots and statistical tests were performed in the R statistical environment version 4.1.0 [38] using different packages [39–47] (See ESM for more details).

Phylogenetic signal

To test for the presence of a phylogenetic signal in our results and visualise the distribution of some of the performance variables measured in our analyses, we built a composite phylogeny based on the publications by [48–50]. See the ESM for additional information on the construction of the tree.

Results

Distribution and fluctuation of stress

Our von Mises stress contour plots for a bite simulated on the lower canine (Figure 1 for von Mises contour plots of a subset of our dataset and Figure S14) show a clear difference between taxa with long and short upper canines. For each angle, regions of high stress are larger (Figure 1) and stress is globally higher (Figure S14) in taxa with shorter canines within the same clade (see *Machairodus aphanistus* vs *Homotherium serum*; *Dinictis felina* vs *Hoplophoneus primaevus*). At a 30° angle, the lowest stress is observed in *Barbourofelis fricki* – the most derived taxa in terms of sabretooth characters[3] – and the highest in the extant *Caracal caracal* (Figure 1 and Figure S14). Globally, felids display higher stress and larger high-stress areas than nimravids. In taxa with short upper canines, there is a high stress area in the coronoid process of the working side at a 30° angle, this stress being better distributed on the balancing side at 60°. Taxa with long upper canines show a global decrease of the stress at larger angles, yet without important redistribution of stress in other regions of the mandible, except in *Barbourofelis fricki* where the stress is projected more ventrally at larger angles but remains on the working side. While a decrease in global stress is generalised in taxa with the longest upper canines (*Smilodon fatalis, Homotherium crenatidens, Barbourofelis fricki*, etc.), it peaks at 60° in the others (e.g., *Caracal caracal, Panthera tigris, Prionailurus rubiginosus*, etc.) and drops drastically at 90°, although those taxa were not mechanically able to open their jaw at such an angle because of the high coronoid process [13].

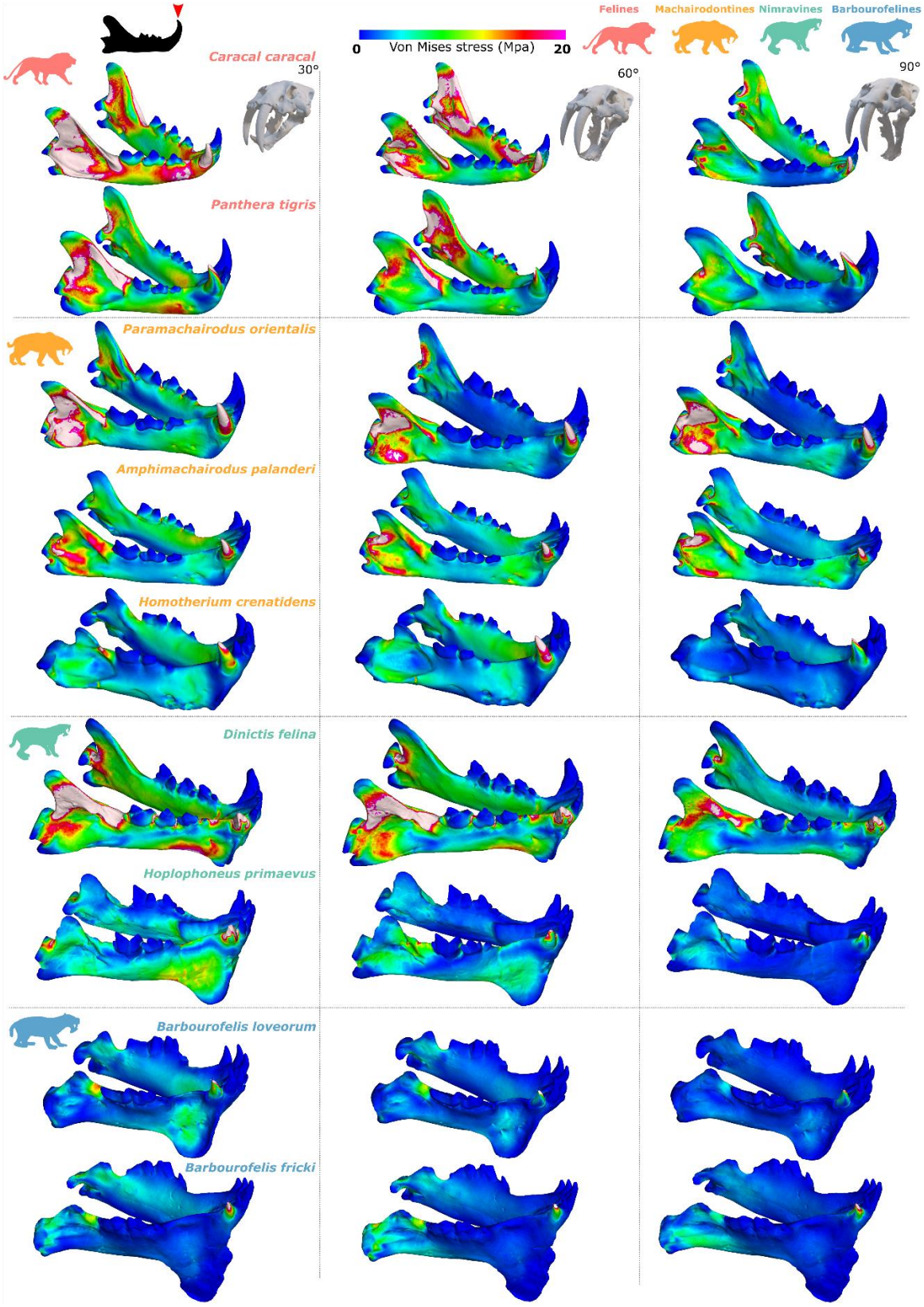

Figure 1: von Mises stress contour plots on nine different taxa at the three different angles for a canine bite. This only show a subset of the complete dataset (17 taxa).

In that sense, early machairodontines (*Paramachaerodus orientalis* and *Machairodus aphanistus*) and taxa considered as 'cheetah-like' taxa (*Yoshi minor*) show a different, 'intermediate' mandibular mechanical behaviour: stress is redistributed on the balancing side at 60° but remains constant on the working side while decreasing on the balancing one at 90°. We obtained little differences when simulating biting on the lower first molar (Figure S15 and Figure S16); the high stress region on the ventral border of the mandible is projected posteriorly on the mandible. In that scenario also, the stress constantly decreases from 30 to 90° degrees in sabretooth taxa while showing a peak at 60° for taxa with shorter upper canines before decreasing at a 90° gape angle. Globally, the stress is higher in smaller taxa and decreases when body size increases within felines (Figure 1; Figure S17-S18).

The evolution of stress across the mandible is somewhat similar for a canine or a molar bite although sometimes slightly higher in molar bite scenarios (e.g., Figure S14A and Figure S15A). Nimravids clearly exhibit lower stress value than felids and felines display higher stress values than machairodontines. The two exceptions in our dataset are *Yoshi minor*, displaying some of the highest stress values recorded (Fig. 2) and *Paramachairodus orientalis*, which shows stress values comparable to those of *Yoshi minor* but solely on the balancing side, at a 30° (see Figure 14B and Figure S14B). The highest stress is usually measured at the base of the coronoid process Figure S14 and Figure S15). In some taxa however (felines, *Yoshi minor* and *Dinictis felina*), stress peaks in the third quarter of the mandible corresponding to a position somewhere below the third lower premolar. While stress is generally extremely low in *Barbourofelis* spp. at a 30° angle it approaches zero at a 90° angle (e.g., minimum measured on the balancing side at 90° for a canine bite 0.18782315). Contrary to what could have been expected the symphysis region does not concentrate lots of stress during the bite; this could be explained by our modelling approach since we did not consider symphyseal material properties, which can have an influence on biomechanical behaviour [51].

Regressions between the stress measured and functional ratio

We test how the von Mises stress correlates with these traits (Figure 2, S19-S21). There is a negative relation between canine length and the mean von Mises stress measured across the mandible for canine (Figure 2) and molar bites (Figure S19); unusual taxa such as *Yoshi minor* and *Prionailurus rubiginosus* undeniably lower the adjusted R squared. There is also a discernible positive relation between coronoid height and von Mises stress, even if again *Yoshi minor* reduces the adjusted R squared (Figure S20 and Figure S21).

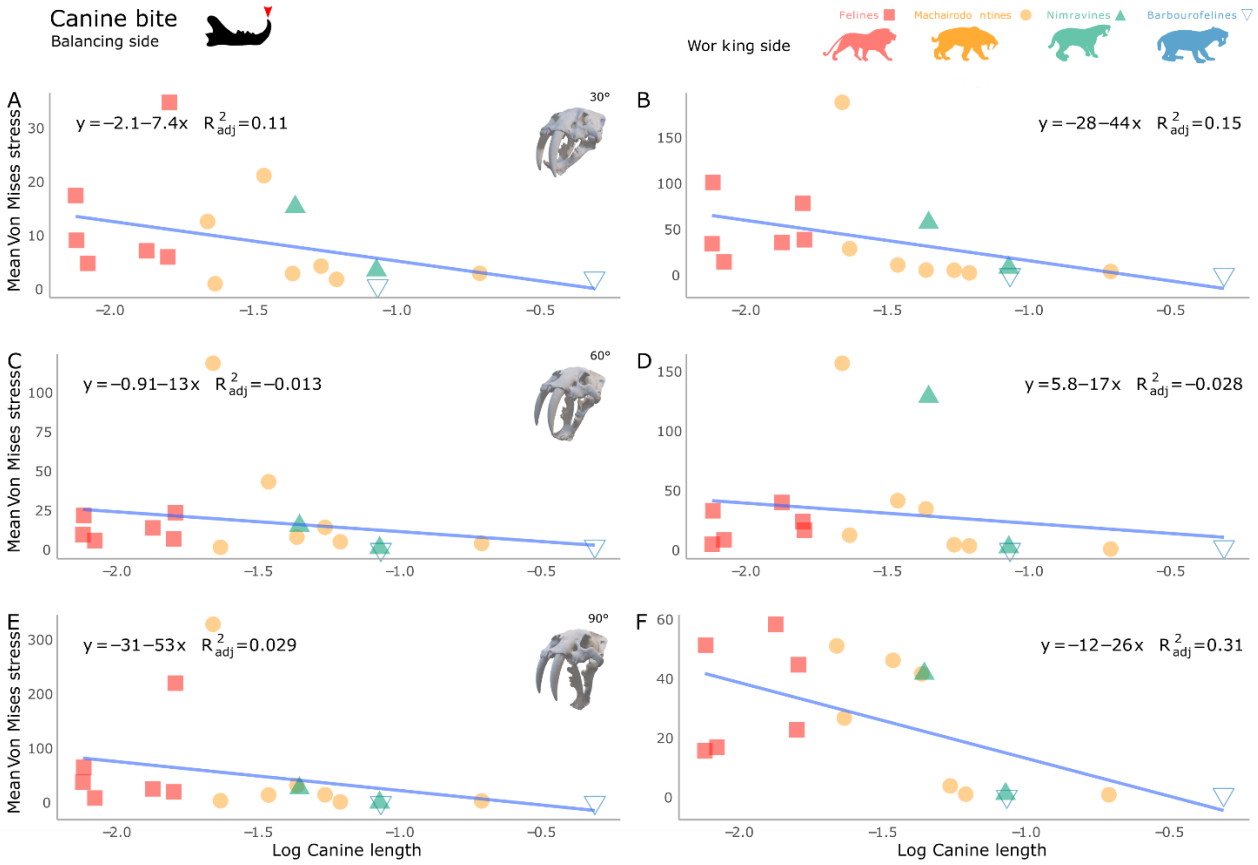

Figure 2: Regressions between the log canine length and the mean von Mises stress measured across the mandible at 30° (A-B), 60° (C-D) and 90° (E-F) for a canine bite in both the balancing (A, C and E) and the working side (B, D and F).

From those plots it is also clear than the mean stress tends to increase at larger angles on the balancing side while it decreases on the working side suggesting an increasing torsion resulting in a destabilisation of the jaw during the bite as previously suggested by [52]. The Phylogenetic generalized linear models shown that the ML estimate was not significantly different from 0, nor from 1 for all the angle tested, on both the balancing and working side. Overall, there is indeed a correlation between the stress in the mandible and the sabretooth trait measured that is not simply due to share ancestry.

Mandible performance

At all the angles measured, both the adjusted strain energy (SE) and mechanical efficiency (ME) are stable in our dataset (Figure S22 and Figure S23). At a 30° angle (Figure S22A-B and Figure S23A), *Barbourofelis fricki* displays the lowest adjusted strain energy in the dataset (below 0.05) while the highest was measured in the machairodontine *Yoshi minor* (from 0.12 to 0.15). Taxa with longer upper canines tend to show lower values of adjusted SE although some extant felines also occupy the low adjusted SE values on the plots (*Panthera tigris*, *Prionailurus rubiginosus*, *Caracal caracal*, and *Lynx rufus*).

Mechanical efficiency is relatively stable in our dataset but it can still be noted that *Smilodon fatalis* explored the widest range of values. At a 60° (Figure S22C-D and Figure S23B), the highest and lowest adjusted strain energy are measured in felines, *Panthera pardus*, and *Prionailurus rubiginosus*, respectively, while there is no clear tendency for the mechanical efficiency. Finally, at the largest gape angle tested (90°) (Figure S22E-F and Figure S23C), the highest adjusted strain energy is measured in *Yoshi minor* and the lowest in the nimravine *Hoplophoneus primaevus*. The nimravine *Dinictis felina* exhibit the highest mechanical efficiency. MANOVA performed on the adjusted strain energy and mechanical efficiency at the three different angles could not recover statistical differences between the families (Felidae and Nimravidae) (p-value at 30° = 0.9718, p-value at 60° = 0.2777, p-value at 90° = 0.0956). Overall, both the adjusted strain energy (Figure S24 and Figure S25) and mechanical efficiency (Figure S26 and Figure S27) decrease at larger gape angles whether for a canine (Figure 3, Figure S24 and Figure S26) or a molar bite (Figure S25 and Figure S27). Furthermore, performance variables (SE and ME) do not correlate with upper canine length (symbolized by the point size on Figure S22 and Figure S23).

The phylogenetic signal for the mechanical efficiency is insignificant for a bite at 30° and 60° but slightly increases at a 90° gape angle. The phylogenetic signal is negligible for the adjusted strain energy at a 30° and 60° bite and remains weak at the 90° bite (Pagel's Lambda and p-values can be seen in Table 2).

Discussion

Our analyses indicate that the sabretooth/non-sabretooth dichotomy is actually weak for mandibles which was already suggested in previous biomechanical simulations [15,16]. Indeed, a first study highlighted functional differences between *Homotherium* and *Smilodon* suggesting different hunting behavior for dirk- and scimitar-toothed cats [15] which is supported by biomechanical analyses on post cranial bones [53]. An even more recent one dealing with a larger dataset [16] highlighted an even greater functional disparity in the cat like mandible showing that metailurins had a mechanical behavior somewhere in between homotherins and pantherins. Globally, species with the longest upper canines are better suited for a bite at larger angles (decreasing von Mises stress values, see Fgure 1 and Figure S15-S17) as previously inferred, but more importantly our new data demonstrate there is no clear dichotomy between 'long upper canines' and 'short upper canines' with instead a continuum of biomechanical responses. Part of this continuum of biomechanical responses is driven by varying stress distribution in the working and balancing side in our dataset highlighting the importance of using both hemimandibles for FEA in order to detect such differences in balancing-working side stress response.

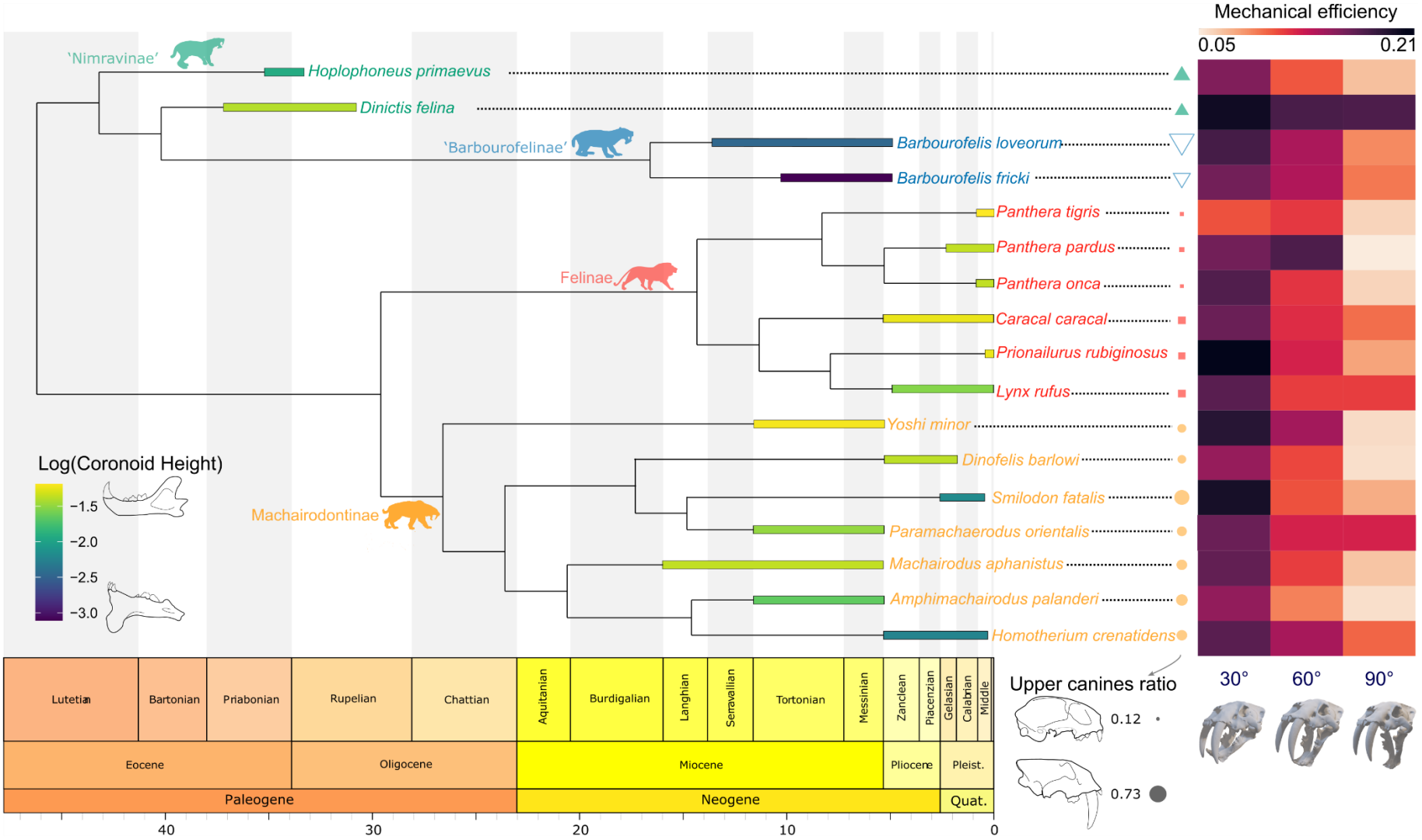

Figure 3: Phylogenetic relationships between the taxa studied with a continuous color scale on the branches indicating the relative coronoid process height on a logarithmic scale, point size indicating the relative upper canine size and a heatmap showing the evolution of mechanical efficiency.

Table 1: Results obtained with the phylosig function for the mechanical efficiency and adjusted strain energy. Phylogenetic signal: None (Low Pagel's Lambda and non-significant P-value), Weak (High Pagel's Lambda or significant P-value), Strong (High Pagel's Lambda and significant P-value)

		Pagel´s Lambda	logL Lambda	p-value	Phylogenetic signal
Mechanical efficiency	30°	6.6107e-05	38. 6404	1	None
	60°	0.102307	35.4671	0.857013	None
	90°	6.6107e-05	26.3708	0.0464958	Weak
Adj. strain energy	30°	6.6107e-05	36.1021	1	None
	60°	6.6107e-05	31.6723	1	None
	90°	0.661484	41.0728	0.385862	Weak

Mandibular stress is reduced at higher gape angles

The canine shear bite has been accepted as the typical sabretooth killing method in opposition to the feline killing bite [6]. However, biomechanical simulations and morphological analyses suggested the existence of an additional, somewhat transitional, and pantherine-like killing method for homotherines and metailurines [16], as well as for the early machairodontines *Machairodus* and *Promegantereon* [17]. Our results demonstrate that some taxa belonging to typical sabretooth clades clearly differ from one another in terms of mandibular von Mises stress, suggesting that some taxa deviated from the canine shear bite and from the feline bite. Distinct mechanical responses are seen in sympatric taxa [54], such as *Hoplophoneus primaevus* + *Dinictis felina; Yoshi minor* + *Amphimachairodus palanderi*, possibly suggesting niche partitioning in feeding mechanics. Also, while the larger gape of sabretooths is usually interpreted as a hunting adaptation to use the elongated upper canines stabilising the prey with the lower canines and incisors [3,6], a consistent drop in stress for lower carnassial bites could suggest that feeding mechanics in sabretooths is also more favourable at higher gapes. In other words, mandibular modifications of sabretooths may also have passively favoured carnassial food processing at larger gapes as well, not solely canine killing bites.

Shorter coronoid process means larger gape and less stress

Within felines, the von Mises stress measured in the mandible was higher in smaller taxa within the same clade, which is not especially the case in other

previous FEA studies, e.g., in otters [26], ungulates [55], or lizards [56]. It was already noted [11] that the largest amount of skull shape variation in felines is driven by allometry over functional or phylogenetic factors while in sabretooths the best predictor was canine length over body size [11]. Extant felids are mostly solitary ambush predators (except for the lion, *Panthera leo*) that bite their prey either in the throat, neck or sometimes the skull [57,58]. In this context, larger gapes expand the range of possible prey size, although field studies show that large species do not focus exclusively on large prey [59]. In extant taxa, gape angle tends to increase non-linearly with body size; the largest species appearing 'overbuilt' [60], in order to allow submission of large, energetic prey. Our results followed the same allometric relationship, as the crania of large feline taxa handle stress better than the smaller ones. Indeed, in our dataset smaller felines (e.g., *Prionailurus rubiginosus*, *Caracal caracal*) have more gracile mandibles than the largest ones (e.g., *Panthera tigris*, *Panthera onca*) which clearly have an impact on the biomechanical behaviour of the mandible as seen in our von Mises stress contour plots (Figure 1). There is a visible relationship between von Mises stress and upper canine height or coronoid process height (Figure 2 and Figure S19–S21), whose *R* squared values are affected by a couple of unusual taxa [11]. This actually contradicts a previous study using 2D biomechanical simulations on cat like mandibles that shown that stress is higher in sabretoothed in the coronoid process but this could be explained by the different models used (2D data extracted from pictures or 3D models) [19]. Also, sabretoothed taxa better handle the torsion induced when biting at large gape with low values of stress on the balancing side which may be explained by the reduction of the size of the coronoid processes and general mandibular shape (Figure 1). However, our dataset is not suited to fully test this assumption and specific tests would have to be done by including the modelling of mandibular symphysis materials, which are key to understand how torsional forces are transferred between hemimandibles [61]. Interestingly, the presence and development of the mandibular flange do not seem to affect any of the performance variables measured in our analyses, thereby questioning its functional importance in biting. It was suggested quite early (see [62]) that those flanges protected the upper canines from lateral pression when the jaw was closed. Our analyses showing that it has no implication during biting could support this assumption although this still does not explain why taxa with extremely elongated upper canines like *Smilodon* do not exhibit such flanges. Surprisingly, the von Mises stress values of felines strongly decreases at a 90° angle while this gape is mechanically impossible in this clade due to the size of the coronoid process and the curvature of post glenoid processes. The decline in stress values in all taxa at a 90° can be perhaps simply explained by the position of the biting points and the orientation of the muscle

pulling the mandible resulting in a moderate stress in the mandibular corpus due to the poor lever arm. At 90°, the muscle vectors have a better alignment with the long axis of the mandible. Thus, sabretooths did not necessarily need specialized morphology to make the mandible any stronger at high gape; the main morphological change was instead to reduce the coronoid process to allow such jaw opening.

Efficiency and strain energy are insensitive to sabretooth morphology

It is almost impossible to differentiate clades (Felines, machairodontines, nimravines, or barbourofelines), families (Felids or nimravids), and morphotypes (sabretooth vs non sabretooth) based on their adjusted strain energy (adj SE), their mechanical efficiency (ME), at the different angles or in the pattern of evolution of ME and adj SE from 30° to 90° (Figure 3 and Figure S21-S26; see MANOVA results above). A weak phylogenetic signal is present in our mechanical efficiency and adjusted strain at a 90° bite (Table 2) possibly due to the particularly high ME in barbourofelines at this gape. This means in effect that mandibular performance is insensitive to sabretooth morphology or phylogenetic relationships.

This unexpected result is particularly important because a wide series of unrelated clades have evolved elongated upper canines, ever since the Permian. When carnivorous, these taxa are often called sabretooth (e.g., thylacosmilids, gorgonopsians, biarmosuchians, anteosaurid dinocephalians) but many other clades have evolved comparable dental morphologies, such as the extant musk deer, chevrotains, the walrus, the Eocene, rhino-like Uintatheriidae [2,4,16,63–67], even bony fish [68]. The potential functions of elongated canines or caniniform teeth range from display, defence, intraspecific aggression, sexual selection, manipulation of food, and the hunting of large prey items [2]. While the exact function remains obscure for some clades, especially in herbivorous extinct taxa [69], the presence of sabre teeth in carnivorous animals is often presented as an adaptation to kill large prey [2,3]. This wide array of possible functions indicates that multiple evolutionary drivers channelled the acquisition of elongated canines. Our results markedly add to this complexity by demonstrating a functional decoupling between canine elongation and mandible performance in the iconic sabretoothed carnivoran mammals.

Finally, as predicted by [70] the ‘many-to-one mapping’ of form-function relationships can be applied to various complex biological systems; the cat-like mandible now appears as a striking example of such a phenomenon, displaying a high morphological disparity with little mechanical variation in terms of mechanical efficiency and adjusted strain energy. This was not expected after the results published by [16] were all the analysed functional parameters (actual and effective gape angle, bending strength, bite force) shown a continuum distribution of results between the two

morphotypes. The similarities in terms of mechanical efficiency and adjusted strain energy could be due to similar canine clearance during the bite. Indeed, forms with smaller upper canines biting at a 30° angle might have a similar canine clearance to extremely derived sabretooth like *Smilodon fatalis* or *Barbourofelis fricki* at a 90° gape angle. Still, our results highlighted a continuum in terms of stress distribution in the cat like mandible possibly suggesting a wide range of hunting methods in those carnivorans.

Conclusions

We thoroughly analysed the biomechanical behaviour of mandibles of cat-like taxa, extant and extinct, under multiple biting scenarios. Our analyses show a better stress repartition in taxa with long upper canines with a global stress decreasing at larger gape angles which corroborate that those species are adapted to bite at larger angles. However, we show a continuous spectrum of mechanical responses in terms of mechanical efficiency and adjusted strain energy in the cat like mandibles rather than a discrete difference between sabretooth and non-sabretooth forms. Despite striking morphological differences within felines, machairodontines, nimravines, and barboroufelines, their mandibular architectures react similarly in a mechanical efficiency and strain energy framework. This indicates a spectrum of hunting methods in cat-like carnivorans rather than a two-peaked adaptive landscape, as forces involved in those different hunting scenarios were not drastically variable. Also, this points out that the cat-like mandible in its non-sabretooth forms was already mechanically strong and able to endure a bite at an extremely large angle (90°) meaning that all the morphological variations associated with the sabretooth ecomorphs are only meant to make that bite possible and not to build a stronger mandible to support that bite.

Authors' contributions

NC, VF, and ZJT designed the study. ZJT collected CT scan data. NC collected laser scan data. NC processed the 3D models, carried out the FE analyses, analysed the data, and drafted the figures and manuscript. All authors contributed to writing the manuscript and gave final approval for publication.

Data availability statement

All 3D models used to perform the finite element analysis are available on MorphoSource (Project ID: 000473875, https://www.morphosource.org/projects/000473875/)

Excel files containing the model properties, raw results, calculation of the adjusted strain energy and mechanical efficiency, final Strand7 loaded files, the modified MATLAB code as well as the R script used to create the plots and perform the statistical tests are provided

as supplementary files and are available on Orbi, the ULiège Open Repository (https://hdl.handle.net/2268/296076).

Funding

NC is supported by a grant of Fonds de la Recherche Scientifique F.R.S.–FNRS (FRIA grant number FRIA FC 36251). VF is supported by a grant of Fonds de la Recherche Scientifique F.R.S.–FNRS (MIS F.4511.19). ZJT is supported by NSF DBI 2128146.

Acknowledgments

We are extremely thankful to all curators, collection managers and staff, whose help and support was fundamental to collect all the scans we needed to perform this study. Especially, we would like to thank: Geraldine Véron (MNHN, Paris, France), Daniela Kalthoff and Thomas Mörs (NRM, Stockholm, Sweden), Benjamin Kear (PMU, Upssala, Sweden), Roula Pappa and Pip Brewer (NHMUK, London, United Kingdom), Patricia Holroyd (UCMP, Berkeley, USA), Samuel A. McLeod and Xiaoming Wang (NHMLA, Los Angeles).

We would also like to show our gratitude to Florent Goussard and Christine Argot (MNHN, Paris, France) for providing us structured light scan and CT scans of *Homotherium crenatidens*. For access to the surface scan data of *Dinofelis barlowi*, we thank the Ditsong National Museum of Natural History, South Africa, and Justin Adams of the Department of Anatomy and Developmental Biology, Monash University, Australia. We are also extremely thankful to Jeanette Pirlo and Sierra Steely for the surface scans of the holotype of *Barbourofelis loveorum* from the University of Florida.

We are immensely grateful to Romain Boman from the Aerospace & Mechanical Engineering department in the University of Liège for his help to improve the forces distribution in the “Boneload” MATLAB routine. Finally, we would like to thank John Hutchinson as well as three anonymous reviewers for their constructive comments on a previous version of the manuscript.

References

1. Turner A, Antón M, Salesa MJ, Morales J. 2011 Changing ideas about the evolution and functional morphology of Machairodontine felids. *Estudios Geologicos* **67**, 255–276. (doi:10.3989/egeol.40590.188)
2. Anton M. 2013 *Sabertooth*. Bloomington: Indiana University Press.
3. Emerson SB, Radinsky L. 1980 Functional analysis of sabertooth cranial morphology. *Paleobiology* **6**, 295–312. (doi:10.1017/S0094837300006813)
4. van Valkenburgh B, Jenkins I. 2002 Evolutionary Patterns in the History of Permo-Triassic and Cenozoic Synapsid Predators. *The Paleontological Society Papers* **8**, 267–288. (doi:10.1017/s1089332600001121)
5. Gonyea WJ. 1976 Adaptive differences in the body proportions of large felids. *Acta Anat (Basel)* **96**, 81–96. (doi:10.1159/000144663)
6. Akersten WA. 1985 Canine function in Smilodon (Mammalia, Felidae, Machairodontinae). *Contributions in Science* , 1–22.
7. Turner A, Antón M. 1997 *The big cats and their fossil relatives: an illustrated guide to their evolution and natural history*. Columbia University Press.
8. Antón M, Galobart À. 1999 Neck function and predatory behavior in the scimitar toothed cat Homotherium latidens (Owen). *J Vertebr Paleontol* **19**, 771–784. (doi:10.1080/02724634.1999.10011190)
9. Argot C. 2004 Functional-adaptive features and palaeobiologic implications of the postcranial skeleton of the late miocene sabretooth borhyaenoid thylacosmilus atrox (Metatheria). *Alcheringa* **28**, 229–266. (doi:10.1080/03115510408619283)
10. Andersson K, Norman D, Werdelin L. 2011 Sabretoothed carnivores and the killing of large prey. *PLoS One* **6**. (doi:10.1371/journal.pone.0024971)
11. Slater GJ, van Valkenburgh B. 2008 Long in the tooth: evolution of sabertooth cat cranial shape. *Paleobiology* **34**, 403–419. (doi:10.1666/07061.1)
12. Martin LD, Babiarz JP, Naples VL, Hearst J. 2000 Three ways to be a saber-toothed cat. *Naturwissenschaften* **87**, 41–44. (doi:10.1007/s001140050007)
13. Matthew WD. 1910 The phylogeny of the felidae. *Bull Am Mus Nat Hist* **28**, 289–318. (doi:10.1007/bf01798035)
14. Figueirido B, MacLeod N, Krieger J, de Renzi M, Pérez-Claros JA, Palmqvist P. 2011 Constraint and adaptation in the evolution of carnivoran skull shape. *Paleobiology* **37**, 490–518. (doi:10.1666/09062.1)

15. Figueirido B, Lautenschlager S, Pérez-Ramos A, van Valkenburgh B. 2018 Distinct Predatory Behaviors in Scimitar- and Dirk-Toothed Sabertooth Cats. *Current Biology* **28**, 3260-3266.e3. (doi:10.1016/j.cub.2018.08.012)

16. Lautenschlager S, Figueirido B, Cashmore DD, Bendel EM, Stubbs TL. 2020 Morphological convergence obscures functional diversity in sabre-toothed carnivores: Sabre-tooth functional morphology. *Proceedings of the Royal Society B: Biological Sciences* **287**. (doi:10.1098/rspb.2020.1818)

17. Chatar N, Fischer V, Siliceo G, Antón M, Morales J, Salesa MJ. 2021 Morphometric Analysis of the Mandible of Primitive Sabertoothed Felids from the late Miocene of Spain Madrid. *J Mamm Evol* **28**, 753–771. (doi:10.1007/s10914-021-09541-0)

18. McHenry CR, Wroe S, Clausen PD, Moreno K, Cunningham E. 2007 Supermodeled sabercat, predatory behavior in Smilodon fatalis revealed by high-resolution 3D computer simulation. *Proc Natl Acad Sci U S A* **104**, 16010–16015. (doi:10.1073/pnas.0706086104)

19. Piras P, Maiorino L, Teresi L, Meloro C, Lucci F, Kotsakis T, Raia P. 2013 Bite of the cats: Relationships between functional integration and mechanical performance as revealed by mandible geometry. *Syst Biol* **62**, 878–900. (doi:10.1093/sysbio/syt053)

20. Janis CM, Figueirido B, DeSantis L, Lautenschlager S. 2020 An eye for a tooth: Thylacosmilus was not a marsupial '"saber-tooth predator"'. *PeerJ* **2020**, 1–36. (doi:10.7717/peerj.9346)

21. Bourke J, Wroe S, Moreno K, McHenry C, Clausen P. 2008 Effects of gape and tooth position on bite force and skull stress in the dingo (Canis lupus dingo) using a 3-dimensional finite element approach. *PLoS One* **3**. (doi:10.1371/journal.pone.0002200)

22. Christiansen P. 2007 Comparative bite forces and canine bending strength in feline and sabretooth felids: Implications for predatory ecology. *Zool J Linn Soc* **151**, 423–437. (doi:10.1111/j.1096-3642.2007.00321.x)

23. Oldfield CC, Mchenry CR, Clausen PD, Chamoli U, Parr WCH, Stynder DD, Wroe S. 2012 Finite element analysis of ursid cranial mechanics and the prediction of feeding behaviour in the extinct giant Agriotherium africanum. *J Zool* **286**, 171–171. (doi:10.1111/j.1469-7998.2011.00862.x)

24. Cox PG, Rinderknecht A, Blanco RE. 2015 Predicting bite force and cranial biomechanics in the largest fossil rodent using finite element analysis. *J Anat* **226**, 215–223. (doi:10.1111/joa.12282)

25. Tseng ZJ, Grohé C, Flynn JJ. 2016 A unique feeding strategy of the extinct marine mammal kolponomos: Convergence on sabretooths and sea otters. *Proceedings of the Royal Society B: Biological Sciences* **283**. (doi:10.1098/rspb.2016.0044)

26. Tseng ZJ, Su DF, Wang X, White SC, Ji X. 2017 Feeding capability in the extinct giant Siamogale melilutra and comparative mandibular biomechanics of living Lutrinae. *Scientific Reports* **7**, 1–10. (doi:10.1038/s41598-017-15391-9)

27. Lautenschlager S, Gill P, Luo ZX, Fagan MJ, Rayfield EJ. 2017 Morphological evolution of the mammalian jaw adductor complex. *Biological Reviews* **92**, 1910–1940. (doi:10.1111/brv.12314)

28. Püschel TA, Marcé-Nogué J, Gladman JT, Bobe RR, Sellers WI. 2018 Inferring locomotor behaviours in Miocene New World monkeys using finite element analysis, geometric morphometrics and machine-learning classification techniques applied to talar morphology. *J R Soc Interface* **15**. (doi:10.1098/rsif.2018.0520)

29. Rowe AJ, Rayfield EJ. 2022 The efficacy of computed tomography scanning versus surface scanning in 3D finite element analysis. *PeerJ* **10**, e13760. (doi:10.7717/PEERJ.13760/SUPP-1)

30. Wroe S, McHenry C, Thomason J. 2005 Bite club: comparative bite force in big biting mammals and the prediction of predatory behaviour in fossil taxa. *Proceedings of the Royal Society B: Biological Sciences* **272**, 619–625. (doi:10.1098/RSPB.2004.2986)

31. Dessem D, Druzinsky RE. 1992 Jaw-muscle activity in ferrets, Mustela putorius furo. *J Morphol* **213**, 275–286. (doi:10.1002/jmor.1052130211)

32. Currey JD. 1987 The evolution of the mechanical properties of amniote bone. *J Biomech* **20**, 1035–1044. (doi:10.1016/0021-9290(87)90021-2)

33. Currey JD, Brear K. 1990 Hardness, Young's modulus and yield stress in mammalian mineralized tissues. *J Mater Sci Mater Med* **1**, 14–20. (doi:10.1007/BF00705348)

34. Gill PG, Purnell MA, Crumpton N, Brown KR, Gostling NJ, Stampanoni M, Rayfield EJ. 2014 Dietary specializations and diversity in feeding ecology of the earliest stem mammals. *Nature* **512**, 303–305. (doi:10.1038/nature13622)

35. Erickson GM, Catanese J, Keaveny TM. 2002 Evolution of the biomechanical material properties of the femur. *Anatomical Record* **268**, 115–124. (doi:10.1002/ar.10145)

36. Grosse IR, Dumont ER, Coletta C, Tolleson A. 2007 Techniques for modeling muscle-induced forces in finite element models of skeletal structures. *Anatomical Record* **290**, 1069–1088. (doi:10.1002/ar.20568)

37. Dumont ER, Davis JL, Grosse IR, Burrows AM. 2011 Finite element analysis of performance in the skulls of marmosets and tamarins. *J Anat* **218**, 151–162. (doi:10.1111/j.1469-7580.2010.01247.x)

38. R Core Team. 2021 R: A language and environment for statistical computing.

39. Wickham H. 2007 Reshaping Data with the reshape Package. *J Stat Softw* **21**.

40. Zeileis A, Grothendieck G, Ryan JA, Ulrich JM, Andrews F. 2022 Package 'zoo'.

41. Revell LJ. 2012 phytools: An R package for phylogenetic comparative biology (and other things). *Methods Ecol Evol* **3**, 217–223. (doi:10.1111/j.2041-210X.2011.00169.x)

42. Bapst DW. 2012 paleotree: an R package for paleontological and phylogenetic analyses of evolution. *Methods Ecol Evol* **3**, 803–807. (doi:10.1111/j.2041-210X.2012.00223.x)

43. Bell MA, Lloyd GT. 2015 strap: an R package for plotting phylogenies against stratigraphy and assessing their stratigraphic congruence. *Palaeontology* **58**, 379–389. (doi:10.1111/PALA.12142)

44. Yu G, Smith DK, Zhu H, Guan Y, Lam TTY. 2017 ggtree: an r package for visualization and annotation of phylogenetic trees with their covariates and other associated data. *Methods Ecol Evol* **8**, 28–36. (doi:10.1111/2041-210X.12628)

45. Wickham H. 2006 An introduction to ggplot: An implementation of the grammar of graphics in R. *Statistics (Ber)* , 1–8.

46. Kassambara A. 2020 ggpubr.

47. Paradis E, Schliep K. 2019 Ape 5.0: An environment for modern phylogenetics and evolutionary analyses in R. *Bioinformatics* **35**, 526–528. (doi:10.1093/bioinformatics/bty633)

48. Barrett PZ. 2021 The largest hoplophonine and a complex new hypothesis of nimravid evolution. *Sci Rep* **11**, 1–9. (doi:10.1038/s41598-021-00521-1)

49. Jiangzuo Q, Werdelin L, Sun Y. 2022 A dwarf sabertooth cat (Felidae : Machairodontinae) from Shanxi , China , and the phylogeny of the sabertooth

tribe Machairodontini. *Quat Sci Rev* **284**, 107517. (doi:10.1016/j.quascirev.2022.107517)

50. Slater GJ, Friscia AR. 2019 Hierarchy in adaptive radiation: A case study using the Carnivora (Mammalia). *Evolution (N Y)* **73**, 524–539. (doi:10.1111/evo.13689)

51. Tseng ZJ, Stynder D. 2011 Mosaic functionality in a transitional ecomorphology: Skull biomechanics in stem Hyaeninae compared to modern South African carnivorans. *Biological Journal of the Linnean Society* **102**, 540–559. (doi:10.1111/j.1095-8312.2010.01602.x)

52. Greaves WS. 1982 A Mechanical Limitation on the Position of the Jaw Muscles of Mammals: The One-Third Rule. *J Mammal* **63**, 261–266. (doi:10.2307/1380635)

53. Anyonge W. 1996 Locomotor behaviour in Plio-Pleistocene sabre-tooth cats: a biomechanical analysis. *J Zool* **238**, 395–413. (doi:10.1111/J.1469-7998.1996.TB05402.X)

54. Van Valkenburgh B. 1999 Major patterns in the history of carnivorous mammals. *Annu Rev Earth Planet Sci* **27**, 463–493. (doi:10.1146/annurev.earth.27.1.463)

55. Zhou Z, Winkler DE, Fortuny J, Kaiser TM, Marcé-Nogué J. 2019 Why ruminating ungulates chew sloppily: Biomechanics discern a phylogenetic pattern. *PLoS One* **14**, e0214510. (doi:10.1371/JOURNAL.PONE.0214510)

56. McCurry MR, Mahony M, Clausen PD, Quayle MR, Walmsley CW, Jessop TS, Wroe S, Richards H, McHenry CR. 2015 The Relationship between Cranial Structure, Biomechanical Performance and Ecological Diversity in Varanoid Lizards. *PLoS One* **10**, e0130625. (doi:10.1371/JOURNAL.PONE.0130625)

57. Ewer RF. 1998 *The Carnivores*. Cornell University Press.

58. Leyhausen P. 1979 *Cat behaviour. The predatory and social behaviour of domestic and wild cats.* First Edition. Garland STPM Press.

59. Radloff FGT, Du Toit JT. 2004 Large predators and their prey in a southern African savanna: a predator's size determines its prey size range. *Journal of Animal Ecology* **73**, 410–423.

60. Slater GJ, Van Valkenburgh B. 2009 Allometry and performance: The evolution of skull form and function in felids. *J Evol Biol* **22**, 2278–2287. (doi:10.1111/j.1420-9101.2009.01845.x)

61. Tseng ZJ, Stynder D. 2011 Mosaic functionality in a transitional ecomorphology: skull biomechanics in stem Hyaeninae compared to modern South African carnivorans. *Biological Journal of the Linnean Society* **102**, 540–559. (doi:10.1111/j.1095-8312.2010.01602.x)

62. Berryman Scott W, Lowell Jepsen G. 1936 The Mammalian Fauna of the White River Oligocene: Part I. Insectivora and Carnivora. *Transactions of the American Philosophical Society* **28**, 1–153.

63. Bubenik GA, Bubenik AB. 1990 *Horns, Pronghorns, and Antlers*. Springer New York. (doi:10.1007/978-1-4613-8966-8)

64. Ivakhnenko MF. 2008 Cranial morphology and evolution of Permian Dinomorpha (Eotherapsida) of eastern Europe. *Paleontological Journal* **42**, 859–995. (doi:10.1134/S0031030108090013)

65. Ivakhnenko MF. 2005 Morphology of the Gorgonopidae (Eotherapsida) and Tetrapod communities in the Late Paleozoic. *Paleontological Journal* **39**, S393–S511.

66. Rubidge BS, Sidor CA. 2001 Evolutionary Patterns among Permo-Triassic Therapsids. *Annu Rev Ecol Syst* **32**, 449–480.

67. Leinders JJM, Heintz E. 1980 Historical notes on the taxonomy and nomenclature of the recent Rhinocerotidae (Mammalia, Perissodactyla). *Beaufortia* **30**, 155–160.

68. Capobianco A, Beckett HT, Steurbaut E, Gingerich PD, Carnevale G, Friedman M. 2020 Large-bodied sabre-toothed anchovies reveal unanticipated ecological diversity in early Palaeogene teleosts. *R Soc Open Sci* **7**, 192260. (doi:10.1098/rsos.192260)

69. Cisneros JC, Abdala F, Rubidge BS, Dentzien-Dias PC, de Oliveira Bueno A. 2011 Dental occlusion in a 260-million-year-old therapsid with saber canines from the permian of Brazil. *Science (1979)* **331**, 1603–1605. (doi:10.1126/science.1200305)

70. Wainwright PC, Alfaro ME, Bolnick DI, Husley CD. 2005 Many-to-One Mapping of Form to Function: A General Principle in Organismal Design? *Integr Comp Biol* **45**, 256–262. (doi:10.1093/icb/45.2.256)